APL Materials

Measurement of local optomechanical properties of a direct bandgap 2D semiconductor

Cite as: APL Mater. **7**, 101126 (2019); https://doi.org/10.1063/1.5117259
Submitted: 30 June 2019 . Accepted: 10 October 2019 . Published Online: 29 October 2019

F. A. Benimetskiy, V. A. Sharov, P. A. Alekseev, V. Kravtsov, K. B. Agapev, I. S. Sinev, I. S. Mukhin, A. Catanzaro, R. G. Polozkov, E. M. Alexeev, A. I. Tartakovskii, A. K. Samusev, M. S. Skolnick, D. N. Krizhanovskii, I. A. Shelykh, and I. V. Iorsh

Measurement of local optomechanical properties of a direct bandgap 2D semiconductor

Cite as: APL Mater. 7, 101126 (2019); doi: 10.1063/1.5117259
Submitted: 30 June 2019 • Accepted: 10 October 2019 •
Published Online: 29 October 2019

F. A. Benimetskiy,[1,a] V. A. Sharov,[2,3] P. A. Alekseev,[2] V. Kravtsov,[1] K. B. Agapev,[1] I. S. Sinev,[1] I. S. Mukhin,[3] A. Catanzaro,[4] R. G. Polozkov,[1] E. M. Alexeev,[4] A. I. Tartakovskii,[4] A. K. Samusev,[1] M. S. Skolnick,[1,4] D. N. Krizhanovskii,[1,4] I. A. Shelykh,[1,5] and I. V. Iorsh[1]

AFFILIATIONS

[1] Department of Physics and Engineering, ITMO University, St. Petersburg 197101, Russia
[2] Ioffe Institute, St. Petersburg 194021, Russia
[3] St. Petersburg Academic University, St. Petersburg 194021, Russia
[4] Department of Physics and Astronomy, University of Sheffield, Sheffield S3 7RH, United Kingdom
[5] Science Institute, University of Iceland, Reykjavik IS-107, Iceland

[a] **Electronic mail:** fedor.benimetskiy@metalab.ifmo.ru

ABSTRACT

Strain engineering is a powerful tool for tuning physical properties of 2D materials, including monolayer transition metal dichalcogenides (TMDs)—direct bandgap semiconductors with strong excitonic response. Deformation of TMD monolayers allows inducing modulation of exciton potential and, ultimately, creating single-photon emitters at desired positions. The performance of such systems is critically dependent on the exciton energy profile and maximum possible exciton energy shift that can be achieved under local impact until the monolayer rupture. Here, we study the evolution of two-dimensional exciton energy profile induced in a $MoSe_2$ monolayer under incremental local indentation until the rupture. We controllably stress the flake with an atomic force microscope tip and perform *in situ* spatiospectral mapping of the excitonic photoluminescence in the vicinity of the indentation point. In order to accurately fit the experimental data, we combine numerical simulations with a simple model of strain-induced modification of the local excitonic response and carefully account for the optical resolution of the setup. This allows us to extract deformation, strain, and exciton energy profiles obtained at each indentation depth. The maximum exciton energy shift induced by local deformation achieved at 300 nm indentation reaches the value of 36.5 meV and corresponds to 1.15% strain of the monolayer. Our approach is a powerful tool for *in situ* characterization of local optomechanical properties of 2D direct bandgap semiconductors with strong excitonic response.

In recent years, single-layer transition metal dichalcogenides (TMDs), 2D direct bandgap semiconductors, have attracted focused attention due to their unique electronic and optical properties.[1] Mechanical strain is an important degree of freedom for wide-range tuning of carrier mobility,[2] bandgap,[3] exciton energy,[4] and other properties in TMDs.[5] This becomes possible since TMDs can sustain homogeneous mechanical strain as large as 10% without rupturing.[6] Strain-induced effects in TMD materials have been comprehensively studied via macroscopic bending, stretching, or compressing the hosting substrate.[5]

Furthermore, the planar geometry of TMDs provides a unique opportunity to use local strain for creating controllable exciton energy profiles and single-photon emitters through 3D quantum confinement of carriers.[7–9] Such "artificial atoms" can be precisely positioned and arranged in lattices by, e.g., transferring TMDs on nanopatterned substrates.[10,11] Another way to realize modulation of exciton energy profile and single-photon sources is non-reversible nanoindentation of a TMD monolayer deposited on a deformable polymer substrate with an atomic force microscope (AFM) probe.[12]

Although the physical position of single-photon emitters is often correlated with areas of local strain,[8,12] the detailed origin of quantum emission in the TMDs remains unclear. Apart from modulating the excitonic potential, local indentation can also lead to a

rupture of the TMD monolayer producing edge and defect states responsible for single-photon emission.[13–16] For future devices supporting on-demand and reversible control of local exciton energy, it is important to distinguish between these two cases as well as obtain critical values of exciton energy shift induced by local deformation before the rupture.

In this work, we use incremental AFM nanoindentation to induce a local modulation of the excitonic properties in a $MoSe_2$ monolayer on a deformable substrate. *In situ* spectral mapping allows us to track the associated modification of the exciton photoluminescence (PL) and, importantly, unambiguously detect the moment of the flake rupture. We use numerical simulations and a simple relation between local strain and emission spectrum to reproduce the whole set of experimental data and reconstruct the deformation and exciton energy profiles realized experimentally under different indentation depths until the rupture. We show that these simulations as well as careful account for the spatial resolution of the optical setup are critical in order to correctly estimate the maximum achieved exciton energy shift, which may otherwise be severely underestimated. Our approach and reconstruction routine are instrumental for *in situ* characterization of local optomechanical properties of TMD-based structures.

Thin-film $MoSe_2$ samples were fabricated by mechanical exfoliation with adhesive tape from a bulk crystal onto a polymer film (Gel-Film® WF ×4 6.0 mil) on top of the SiO_2 substrate [Fig. 1(a)]. Monolayer regions were identified using fluorescence microscopy under 405 nm laser diode illumination through the characteristic increase in the PL signal.[17] The insets in Fig. 1(a) show bright field (left) and PL (right) images of a selected monolayer sample used in our experiment.

The experimental setup is sketched in Fig. 1. We employ indentation by an AFM tip to investigate the fundamental optomechanical properties of locally strained TMD flakes. The tip was intentionally blunted to ~400 nm apex size by focused ion beam milling to avoid early rupturing of the flake and reduce sensitivity of the system under study to the tip shape. After the milling procedure, the tip had a plane facet orthogonal to the indentation direction (parallel to the $MoSe_2$ surface).

Indentation experiments and AFM studies were realized using an AIST SmartSPM™ module with a stiff probe (NT-MDT VIT_P, 50 N/m). During the experiment, the sample topography was controlled using the semicontact (tapping) mode before and after the indentation. Importantly, in the semicontact mode, the impact of the probe on the surface is virtually absent, which allows us to reliably determine the zero indentation point. After this, the indentation was performed in the contact mode (nonoscillating cantilever) by moving the sample piezoscanner along the vertical axis. The precision of the capacitive sensors controlling the piezoscanner was better than 1 nm. The drift of the sample during the indentation was confirmed to be negligible.

Taking into account the very high elasticity of Gel-Film (the film is a polysiloxane-based polymer similar to poly-dimethyl siloxane[18]), the vertical displacement of the sample relative to the stationary cantilever from the tip–sample contact position was directly interpreted as the indentation depth. This assumption is valid only when cantilever bending is negligible in comparison with sample deformation. We further confirmed the absence of cantilever bending from force–distance curves. An indentation of 500 nm led only to a small (sub-10 nm) displacement of the cantilever. At the same time, AFM scan after measuring this force–distance curve showed a permanent indent of the surface indicating its plastic deformation. Additional AFM studies showed that the plastic deformation occurs with indentation depths exceeding 400 nm and further experiments, including PL measurements, were performed with smaller indentation depths where only elastic processes occur. Using a stiff

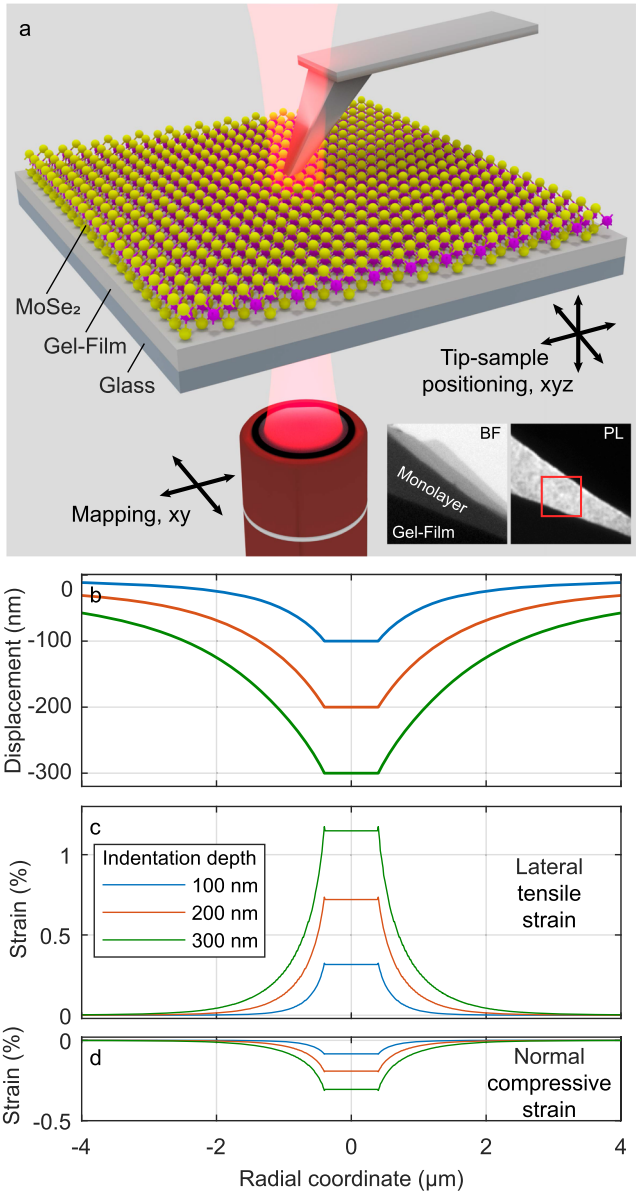

FIG. 1. (a) Schematic of the experimental setup for local strain engineering in TMDs with an atomic force microscope tip. The inset shows bright-field (BF) and photoluminescence (PL) images of the sample. The red square marks the region selected for mapping. [(b)–(d)] Calculated profiles of (b) $MoSe_2$ monolayer vertical displacement, (c) lateral and (d) normal components of strain for different AFM tip indentation depths.

cantilever is advantageous because the indentation depth for further numerical modeling is obtained directly from the piezoscanner capacitive sensors. For softer cantilevers, a nonlinear dependence of the probe–surface contact stiffness during the indentation should be taken into account, which lowers the precision of the extracted indentation value.[19]

We determined the strain of the $MoSe_2$ monolayer associated with the local deformation by an AFM tip by modeling the system in the structural mechanics module of COMSOL Multiphysics. For simplicity, cylindrical symmetry was assumed. The $MoSe_2$ flake was represented by a membrane with a radius of 75 μm and a thickness of 0.7 nm perfectly bonded to a Gel-Film substrate with a radius of 100 μm. Young's moduli for $MoSe_2$ and Gel-Film were chosen as 178 GPa and 0.5 MPa, respectively.[20,21] The simulation results obtained for different AFM tip indentation depths are presented in Figs. 1(b)–1(d), with displacement in (b), lateral strain in (c), and normal strain in (d).

As seen in Fig. 1(b), the deformed region of the $MoSe_2$ flake is much larger than the tip–flake contact region (≈10 μm and ~1 μm in diameter, respectively). This increase in the deformed area in comparison with the AFM tip diameter is due to the very large (10^5) difference in Young's moduli of $MoSe_2$ and Gel-Film and agrees well with the recent results by Niu *et al.*[19] Furthermore, the lateral tensile strain of the membrane [1.15% beneath the tip for the indentation depth of 300 nm, Fig. 1(c)] is ~4 times larger than the normal compressive strain [0.3%, Fig. 1(d)].

For an *in situ* optical characterization of the induced strain profile, we perform spatiospectral mapping of the PL signal for different indentation depths. In the experiment, the sample is excited from the substrate side with 632.8 nm HeNe cw laser light focused with a ×100/0.7 Mitutoyo objective lens. The PL signal is collected with the same objective and analyzed with a Horiba LabRAM spectrometer in a confocal arrangement. To map the spatial distribution of the deformation-driven PL spectral shift, we raster scanned the focal spot of the objective in the sample plane, while both the probe and the sample remained stationary.

The resulting maps of the PL peak position and intensity from a $MoSe_2$ flake for different indentation depths are shown in Figs. 2(a)–2(e) and 2(g)–2(k), respectively. The peak position maps reveal a minor inherent heterogeneity, which can be attributed to the initial tension accumulated during flake transfer onto the Gel-Film. This is confirmed by the corresponding differential maps for the indentation-induced PL peak position shift [Fig. 2(f)] and intensity decrease [Fig. 2(l)]. With increasing indentation depth, the effect of local deformation in the PL intensity maps gradually becomes more apparent [Figs. 2(g)–2(k)]. At the point of tip impact, the observed PL peak exhibits a red-shift and weakens, as quantified in Figs. 3(b) and 3(c) (gray symbols), which is consistent with previous works.[22,23] In the experiment, the maximum measured energy shift and intensity decrease in the PL peak are ~13 meV and 22.3%, respectively, at the 300 nm indentation depth [Figs. 2(f) and 2(l)]. Further increase in the indentation to 350 nm leads to a drastic change in the measured PL map [Figs. 2(e) and 2(k)], where the modulation of the PL intensity and peak position completely disappears as a direct consequence of strain relaxation after the flake rupture. This allows us to unambiguously identify the rupture threshold.

To compare our measured results with theoretically predicted local strain-induced modification of the optical properties of TMDs, we perform density functional theory (DFT)[24] calculations. Within DFT, we self-consistently solve the system of one-electron Kohn–Sham equations[25] and determine the ground state of the system. To take into account the exchange-correlation effects, we use the generalized gradient approximation[26,27] of DFT with Perdew, Burke, and Ernzerhof functional.[28,29] It is local but considers the gradient of electron density as a correction. To describe the exciton excitations in the absorption spectrum, we should solve for the macroscopic dielectric function the Bethe–Salpeter equation (BSE)[30,31] which takes into consideration two particle excitations. This is especially important for a monolayer system due to the weak Coulomb screening and, as a result, strong excitonic effect. The BSE is solved with occupied valence and unoccupied conduction band states obtained by two different ways: one from pure DFT and another from DFT corrected by G_0W_0 approximation, which is single shot *GW* calculation. *GW* approach provides the possibility to take into account the self-energy part that is determined by the sum of the Hartree-like term and Fock-like term, in a single-electron equation (see, for example, Refs. 32 and 33).

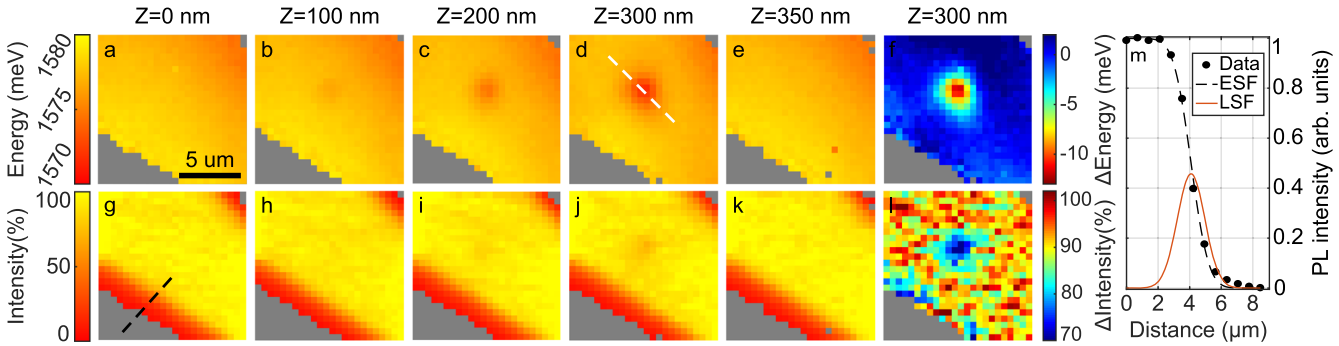

FIG. 2. Maps of the $MoSe_2$ monolayer PL peak energies [(a)–(e)] and peak intensities [(g)–(k)] for different indentation depths (0, 100, 200, 300, and 350 nm). (f) and (l) show the respective differential maps for the 300 nm indentation. (m) PL intensity profile across the $MoSe_2$ edge as indicated by the dashed line in panel (g). The experimental data are shown with dots. The dashed and solid curves represent the edge spread function (ESF) and line spread function (LSF) fits, respectively. The waist of the error function is equal to 1.69 μm as determined by the ESF fit.

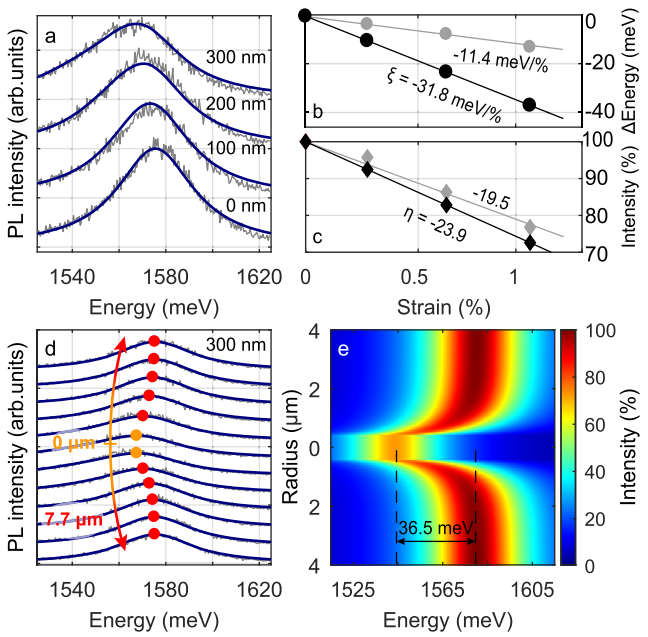

FIG. 3. (a) Measured PL spectra at the tip impact point for different indentation depths (gray curves), together with model fits (blue curves). (b) Exciton peak position and (c) PL intensity as functions of strain. The values obtained directly from PL mapping are shown in gray, while the extracted parameters accounting for the optical resolution are shown in black. (d) PL spectra measured across the deformation region as illustrated by the dashed line in Fig. 2(d). Spectra at the tip impact point are labeled with orange symbols. (e) Strain profile dependence of the modeled spectra for the 300 nm indentation depth.

Our first-principles DFT calculations are performed using the Quantum Espresso package.[34,35] The G_0W_0 correction and the BSE are calculated via the Yambo project package.[36] To solve the BSE and obtain macroscopic dielectric function, the Yambo package applies the Tamm-Dancoff approximation,[37,38] which allows working with Hermitian matrices by neglecting the interaction between quasiparticle pairs. The BSE equation is solved numerically by using the Lanczos–Haydock algorithm[39] with a continued fraction as a result.

As a result of these *ab initio* calculations, we obtain deformation potentials for the exciton energy of −43.5 meV/% and 10 meV/% for lateral stretching and normal compression, respectively. The difference between DFT + BSE and *GW* + BSE results is found to be negligible. The simulated deformation potential for the normal strain is ~4 times smaller than that for the lateral strain. Furthermore, the normal strain in our experimental geometry is ~4 times weaker than lateral strain. Therefore, the normal strain contribution will be neglected in further considerations.

The exciton peak shift obtained directly from PL mapping at the 300 nm indentation depth [Fig. 2(f)] is ~4 times smaller than that predicted theoretically by *ab initio* calculations combined with simulations of strain distribution [see Fig. 1(c)]. This significant discrepancy is primarily due to the limited spatial resolution of the optical setup, as discussed below. In the experiment, the diameter of the effective collection area (diameter w) can be estimated from the PL intensity profile along the direction perpendicular to the flake edge [see Fig. 2(g)]. The measured profile is best fitted by a function $1 - \mathrm{erf}(\sqrt{2}x/w)$, with $w = 1.69$ μm. This resolution is of the order of the spatial scale of the deformation, resulting in significant underestimation of the maximum local peak shift.

In order to account for the optical resolution and extract the optomechanical properties of the TMD monolayer, we first introduce a simple model, which relates the local Lorentzian-shaped PL spectrum with strain in each spatial location. In the linear approximation, we assume that the induced strain results in a linear exciton energy shift and linear PL intensity change with respective coefficients ξ and η [Figs. 3(b) and 3(c)]. We also assume that the spectral width of the exciton PL remains unchanged, which is adequate in the first-order approximation.[4] We reconstruct spectral maps expected in the experiment by spatial convolution of the local spectra calculated for given ξ and η with the Gaussian point spread function [PSF; see Fig. 2(m)].

Figures 3(a) and 3(d) show measured (gray lines) and simulated (blue lines) spectra obtained with the optimized parameters $\xi = -31.8$ meV/% and $\eta = 23.9$. Their direct comparison shows a very good agreement between theory and experiment, confirming our successful reconstruction of the deformation and exciton energy profiles for a dynamically controlled local indentation. Moreover, the obtained value of the deformation potential $\xi = -31.8$ meV/% is well-correlated with our *ab initio* simulations (−43.5 meV/%) and previously reported results for $MoSe_2$ of $\xi = -38$ meV/%[4] and $\xi = -27$ meV/%.[22] The discrepancy in the extracted and simulated deformation potentials most likely originates from the fact that we do not account for a possible small strain-induced change in the linewidth of the exciton PL.[4] Another possible contribution to this discrepancy can be related to the asymmetric shape of the TMD flake used in the measurement, as compared to the symmetric shape assumed in our COMSOL simulations.

Figure 3(b) clearly shows that the deformation potential ξ extracted with account for the optical resolution in our experimental geometry is ~3 times larger than that obtained directly from the measured PL spectrum at the indentation point. This difference is due to the spatial averaging of the inhomogeneously shifted exciton PL spectrum within the collection spot in the experiment. Meanwhile, the factor η responsible for the strain-induced change of PL intensity appears less sensitive to the resolution [see Fig. 3(c)].

Finally, we plot the radial dependence of the local exciton PL spectra corresponding to the maximum indentation depth of $Z = 300$ nm [Fig. 3(e)], achieved before the rupture. As seen from the figure, the maximum exciton energy shift of 36.5 meV is of the order of the PL half-width (38 meV) and greater than the thermal energy of 25.7 meV under ambient conditions. This suggests possibilities to create strain-induced TMD-based quantum emitters for room temperature operation.

To conclude, we develop and demonstrate an approach for an *in situ* characterization of the local optomechanical properties of atomically thin 2D materials. In the experiment, we perform a local indentation of a monolayer $MoSe_2$ flake by an AFM tip with incremental depth until the rupture and carry out *in situ* PL mapping of the indented region. For each indentation depth, we extract the resulting exciton energy profile using a complex approach that combines modeling the spatial distribution of local deformation and careful account of the optical resolution. The rates for the exciton

spectral shift and PL intensity change determined in our experiment are −31.8 meV and 23.9% per 1% of strain, respectively. This is in good agreement with the previous measurements based on macroscopic strain and the results of our *ab initio* simulations. The maximum exciton energy shift induced by local deformation achieved at a 300 nm indentation depth below the rupture threshold reaches the value of 36.5 meV and corresponds to 1.15% strain of the monolayer, suggesting possibilities of creating strain-related TMD exciton potential modulation and quantum emitters for room temperature operation. The proposed complex approach opens new ways for the studies of local optomechanical properties of 2D direct-bandgap semiconductors.

The authors acknowledge funding from the Ministry of Education and Science of the Russian Federation (Megagrant No. 14.Y26.31.0015, Zadanie No. 3.8891.2017/8.9, and Zadanie No. 3.1365.2017/4.6). I. V. Iorsh acknowledges the support of Grant of President of Russian Federation No. MK-6248.2018.2. A.I.T. and D.N.K. acknowledge UK EPSRC Grant No. EP/P026850/1. V.K. acknowledges support from the Government of the Russian Federation through the ITMO Fellowship and Professorship Program.

REFERENCES

[1] K. F. Mak and J. Shan, Nat. Photonics **10**, 216 (2016).
[2] M. Hosseini, M. Elahi, M. Pourfath, and D. Esseni, IEEE Trans. Electron Devices **62**, 3192 (2015).
[3] P. Johari and V. B. Shenoy, ACS Nano **6**, 5449 (2012).
[4] I. Niehues, R. Schmidt, M. Drüppel, P. Marauhn, D. Christiansen, M. Selig, G. Berghäuser, D. Wigger, R. Schneider, L. Braasch *et al.*, Nano Lett. **18**, 1751 (2018).
[5] S. Deng, A. V. Sumant, and V. Berry, Nano Today **22**, 14–35 (2018).
[6] S. Bertolazzi, J. Brivio, and A. Kis, ACS Nano **5**, 9703 (2011).
[7] J. Feng, X. Qian, C.-W. Huang, and J. Li, Nat. Photonics **6**, 866 (2012).
[8] S. Kumar, A. Kaczmarczyk, and B. D. Gerardot, Nano Lett. **15**, 7567 (2015).
[9] G. D. Shepard, O. A. Ajayi, X. Li, X. Zhu, J. Hone, and S. Strauf, 2D Mater. **4**, 021019 (2017).
[10] H. Li, A. W. Contryman, X. Qian, S. M. Ardakani, Y. Gong, X. Wang, J. M. Weisse, C. H. Lee, J. Zhao, P. M. Ajayan *et al.*, Nat. Commun. **6**, 7381 (2015).
[11] A. Branny, S. Kumar, R. Proux, and B. D. Gerardot, Nat. Commun. **8**, 15053 (2017).
[12] M. R. Rosenberger, C. K. Dass, H.-J. Chuang, S. V. Sivaram, K. M. McCreary, J. R. Hendrickson, and B. T. Jonker, ACS Nano **13**, 904 (2019).
[13] C. Chakraborty, L. Kinnischtzke, K. M. Goodfellow, R. Beams, and A. N. Vamivakas, Nat. Nanotechnol. **10**, 507 (2015).
[14] Y.-M. He, G. Clark, J. R. Schaibley, Y. He, M.-C. Chen, Y.-J. Wei, X. Ding, Q. Zhang, W. Yao, X. Xu *et al.*, Nat. Nanotechnol. **10**, 497 (2015).
[15] M. Koperski, K. Nogajewski, A. Arora, V. Cherkez, P. Mallet, J.-Y. Veuillen, J. Marcus, P. Kossacki, and M. Potemski, Nat. Nanotechnol. **10**, 503 (2015).
[16] A. Srivastava, M. Sidler, A. V. Allain, D. S. Lembke, A. Kis, and A. Imamoğlu, Nat. Nanotechnol. **10**, 491 (2015).
[17] P. Tonndorf, R. Schmidt, P. Böttger, X. Zhang, J. Börner, A. Liebig, M. Albrecht, C. Kloc, O. Gordan, D. R. T. Zahn, S. M. de Vasconcellos, and R. Bratschitsch, Opt. Express **21**, 4908 (2013).
[18] A. Castellanos-Gomez, M. Buscema, R. Molenaar, V. Singh, L. Janssen, H. S. J. van der Zant, and G. A. Steele, 2D Mater. **1**, 011002 (2014).
[19] T. Niu, G. Cao, and C. Xiong, Int. J. Solids Struct. **132-133**, 1 (2018).
[20] Y. Yang, X. Li, M. Wen, E. Hacopian, W. Chen, Y. Gong, J. Zhang, B. Li, W. Zhou, P. M. Ajayan *et al.*, Adv. Mater. **29**, 1604201 (2017).
[21] N. Iguiñiz, R. Frisenda, R. Bratschitsch, and A. Castellanos-Gomez, Adv. Mater. **31**, 1807150 (2019).
[22] J. O. Island, A. Kuc, E. H. Diependaal, R. Bratschitsch, H. S. J. van der Zant, T. Heine, and A. Castellanos-Gomez, Nanoscale **8**, 2589 (2016).
[23] J. Liang, J. Zhang, Z. Li, H. Hong, J. Wang, Z. Zhang, X. Zhou, R. Qiao, J. Xu, P. Gao *et al.*, Nano Lett. **17**, 7539 (2017).
[24] P. Hohenberg and W. Kohn, Phys. Rev. **136**, B864 (1964).
[25] W. Kohn and L. J. Sham, Phys. Rev. **140**, A1133 (1965).
[26] S. Kurth, J. P. Perdew, and P. Blaha, Int. J. Quantum Chem. **75**, 889 (1999).
[27] V. N. Staroverov, G. E. Scuseria, J. Tao, and J. P. Perdew, Phys. Rev. B **69**, 075102 (2004).
[28] J. P. Perdew, K. Burke, and M. Ernzerhof, Phys. Rev. Lett. **77**, 3865 (1996).
[29] K. Burke, J. P. Perdew, and Y. Wang, *Electronic Density Functional Theory* (Springer, 1998), pp. 81–111.
[30] E. E. Salpeter and H. A. Bethe, Phys. Rev. **84**, 1232 (1951).
[31] L. X. Benedict and E. L. Shirley, Phys. Rev. B **59**, 5441 (1999).
[32] G. Onida, L. Reining, and A. Rubio, Rev. Mod. Phys. **74**, 601 (2002).
[33] K. Held, C. Taranto, G. Rohringer, and A. Toschi, preprint arXiv:1109.3972 (2011).
[34] P. Giannozzi, J. Phys.: Condens. Matter **21**, 395502 (2009).
[35] P. Giannozzi, O. Andreussi, T. Brumme, O. Bunau, M. B. Nardelli, M. Calandra, R. Car, C. Cavazzoni, D. Ceresoli, M. Cococcioni *et al.*, J. Phys.: Condens. Matter **29**, 465901 (2017).
[36] A. Marini, C. Hogan, M. Grüning, and D. Varsano, Comput. Phys. Commun. **180**, 1392 (2009).
[37] I. Tamm, J. Phys. (USSR) **9**, 449 (1945).
[38] S. Dancoff, Phys. Rev. **78**, 382 (1950).
[39] R. Haydock, Comput. Phys. Commun. **20**, 11 (1980).